Imaging passive seismic data

Brad Artman

brad@sep.stanford.edu

Stanford Exploration Project, Mitchell Building, Department of Geophysics,

Stanford University, Stanford, CA 94305-2215

ABSTRACT

Passive seismic imaging is the process of synthesizing the wealth of subsurface information available from reflection seismic experiments by recording the ambient sound available at the location of an array of geophones distributed at the surface. Cross-correlation of the traces of such a passive experiment synthesizes data of a form that is immediately useful for analysis by the various techniques that have been developed for the manipulation of reflection seismic data.

Passive data is often quite long in order to collect sufficient signal. However, only the very early lags of the correlations need be maintained. Fourier analysis of the windowing of the correlation output reveals that time domain aliasing of the input produces an identical result to windowing the output. This reduces the order of computations by the length of the original trace. However, the aliasing makes the data only usable by a narrow class of migration algorithms which includes shot-profile depth migration.

Migration is an almost universally applied tool to facilitate the interpretation of reflection seismic data. For data acquired in a passive fashion, it is even more important because the source wavefields are likely weak and complex. With a correlation based imaging condition, wave-equation shot-profile

depth migration can use raw passive data as input to produce the same result obtained by preprocessing before migration. Migrating directly also saves the cost of correlations to create shot-gathers.

In the last section, I present images from a shallow passive investigation targeting a buried hollow pipe and the water table reflection. The images show a strong anomaly at the $1m$ depth of the pipe and faint events that could be the water table around $3m$. The images are not so clear as to be irrefutable. A number of deficiencies in the survey design and execution are identified for future efforts.

INTRODUCTION

Passive seismic imaging is an example of wavefield interferometric imaging. In this case, the goal is the production of subsurface structural images by recording the ambient noisefield of the earth with surface arrays of seismometers or geophones. The images produced with this technique are directly analogous to those produced with the conventional reflection seismic experiment with which the geophysical community is so familiar. Within the exploration seismic community, the words imaging and migration are often used synonymously. Likewise, this paper presents the processing of passive seismic data as a migration operation.

The idea of imaging the subsurface without application of a known source was first introduced by Claerbout (1968). That work provides a one-dimensional proof that the auto-correlation of time series collected on the surface of the earth can produce the equivalent to a zero offset time section. Subsequently, Zhang (1989), through plane-wave decomposition, proves the result in 3D over a homogeneous medium. Derode et al. (2003) presents the development of the Green's function of a heterogeneous medium with acoustic waves via correlation as well as an ultrasonic experiment to validate the development. Wapenaar et al. (2004), through one-way reciprocity, prove that by cross-correlating traces of the observed transmission response of a medium, one can synthesize the

complete reflection response, i.e. shot-gathers, collected in a conventional active source experiment. Schuster et al. (2004) shows that the Kirchhoff migration kernel to image correlated gathers is identical to that used to migrate prestack active data when one assumes impulsive virtual sources are located at all the receiver locations. In summary, it is now well established that the difference in time of the arrival of energy at two receivers is informative about the medium through which it passed along the way.

To distinguish data collected passively without the use of active sources from reflection seismic, the former will be transmission wavefields and the latter reflection wavefields. Also to simplify some of the following notation, though not necessary, data are assumed collected on the surface of the earth. One important difference between the two, is that the bulk of the raw data in a transmission wavefield is likely worthless. Useful seismic energy captured in the transmission wavefield could include random distributions of subsurface noise, down-hole sources, or planar teleseismic arrivals. Assuming they are not happening continuously, and not knowing when they occur, the passive seismologist must continuously record. Sampling for high frequencies with large arrays, the problem quickly becomes one of storage space and processing cost even though the mathematics behind making passive data useful is simple.

Transforming transmission wavefields into a more familiar form immediately offers the potential to apply the wealth of processing know-how that has been developed for active seismic surveys to this novel acquisition methodology. Foremost among these options, this paper will explain the benefits of migrating the data in order to increase the signal-to-noise ratio of reflections by mapping signal from all receivers to common subsurface locations. Further, migration provides an output space with higher resolution than the station spacing of the acquisition. After the basic kinematics of the passive experiment are explained, the following section will introduce some of the basics of migration and insert passive seismic processing within the production of the subsurface structural image. Several

synthetic data sets will be then be used to demonstrate these concepts on plausible data constructs. Finally, results from a small field experiment will be presented.

TRANSMISSION TO REFLECTION WAVEFIELDS

Passive seismic imaging is predicated on raypaths bouncing every which-way from every direction. Cartoons depicting the experiment always leave something out that causes an inconsistency that needs more raypaths and receivers to explain. Unfortunately the trend continues nearly forever. Figure 1, simplified for clarity, shows the basic kinematics exploited in processing passively collected data. The figure includes two recording stations capturing an approximately planar wavefront emerging from a two-layer subsurface. Panel (a) shows the ray-paths associated with the direct arrival and one reflected both at the free-surface and the subsurface interface. The second travel path (labeled reflection ray) has the familiar kinematics of the reflection seismic experiment if a source were excited at the location of receiver one. The transmission wavefield is shown in panel (b). Wavelet polarity is appropriate for direct arrivals and reflection. The three main features of the passive data can be appreciated here. First, the exact timing of the energy is unknown. Second, the phase, spectrum, and duration of transmitted energy are unknown and likely complicated. Third, if the incident wavetrain coda is long, arrivals in the transmission record can interfere.

Choosing trace *r1* as the comparison trace, panel (c) depicts the correlation spikes associated with the arrivals in the data panel (b), where $\otimes$ is correlation. A solid line with linear move-out is superimposed across the correlated traces that corresponds to the direct arrival recorded at each receiver location. The dashed line on panel (c) has hyperbolic moveout. However, no correlation peak exists on the $r1 \otimes r1$ trace under the hyperbola. Not drawn, the second arrival on *r2* will have a counterpart on *r1* from a ray reaching the free-surface further to the left of the model. In fact the correlations

produced from a single planewave will produce another planewave.

However, each planar reflection is moved to the lag-time associated with a two-way trip from the surface to the reflector. Correlation removes the wait time for the initial arrival and maintains the time differences between the direct arrival and reflections. Summing the correlations from a full suite of planewaves builds hyperbolic events through constructive and destructive interference. Analyzing seismic data in terms of planewave constituents is a commonly invoked tool in seismic processing. Summing the correlations from incident planewaves is a planewave superposition process.

Correlation returns time differences. The differences between the direct arrival and later reflections are our goal. However, further complication arises with the inclusion of a second reflector. The two reflection rays will correlate with each other with a positive coefficient. The two travel paths share the time through the shallow layer, so they correlate at lag equal to the two-way travel time through the deep layer. This correlation is not a problem however. Part of the energy of the direct arrival will have made an intrabed multiple within the deep layer. This event has the opposite polarity from the direct arrival after once changing its propagation direction from $\uparrow$ to $\downarrow$. The delay of its arrival at receiver *r2* compared to the direct arrival at receiver *r1* is also the two-way travel time of the deep layer. This correlation thus has the same lag as the one between the reflectors and opposite sign.

This shows the importance of multiples within the data to counter potential artifacts of the correlation. Aside from quickly increasing the complexity of simple drawings, it also shows the importance of modeling passive data with a two-way extrapolator. Without all possible multiples, correlation artifacts will quickly overwhelm the earth structure. The destructive interference from multiples in an n-layered earth cancel $2n-1$ false correlations.

Cross-correlation of each trace with every other trace handles the three main difficulties of passive

recordings: timing, waveform, and interference. First, the output of the correlation is in lag units, that when multiplied by the time sampling interval, provide the time delays between like events on different traces. The zero lag of the correlation takes the meaning of zero time for our synthesized shot-gathers. Second, each trace records the character and duration of the incident energy as it is reflected at the surface. This becomes the source wavelet, analogous to a recorded vibrator sweep. Third, overlapping wavelets do not confuse the correlation operator.

To calculate the Fourier transform of the reflection response of the subsurface, $R(\mathbf{x}_r, \mathbf{x}_s, \omega)$, Wapenaar et al. (2004), proves

$$2\Re[R(\mathbf{x}_r, \mathbf{x}_s, \omega)] = \delta(\mathbf{x}_s - \mathbf{x}_r) - \int_{\delta D_m} T(\xi, \mathbf{x}_r, \omega) T^*(\xi, \mathbf{x}_s, \omega)\, \delta^2\xi \ , \tag{1}$$

The vector $\mathbf{x}$ will correspond herein to horizontal coordinates, where subscripts r and s indicate any, different, station locations from a transmission wavefield. After correlation they acquire the meaning of receiver and source locations, respectively, associated with an active survey. The RHS represents summing correlations of windows of passive data around the occurrence of individual sources from three-dimensional locations ξ. The transmission wavefields also need to share a similar notion of time for this formulation as well. This subtlety will be explored in detail below. To synthesize the reflection experiment exactly, impulsive sources should completely surround the volume of the subsurface one is trying to image. Conversely, many impulses can be substituted with of a full suite of plane waves emergent from all angles and azimuths as in the kinematic explanation above.

Time windowing & Fourier subsampling

After correlating passively recorded traces, it is appropriate to discard the lags corresponding to times greater than the two-way travel time to the deepest reflector of interest. Correlation of more than a

few hundred samples is more efficiently performed in the Fourier domain, $C(\omega) = B(\omega)A^*(\omega)$. This operation is linear, so any manipulation of the output could first be performed on the inputs.

Time windowing has a Fourier dual operation. The Fourier sampling theorem, solved for Δt is

$$\Delta t = 1/(N\Delta f)\,.$$

Subsampling the frequency axis increases Δf by a, and reduces the number of samples to N/a. The new time domain trace length is $\Delta t\ N/a$. Removing every other frequency, $a = 2$, halves the length of the trace in the time domain. This process is the symmetric version of reducing the Nyquist frequency by subsampling the time axis.

The left panel of Figure 2 shows a processing flow of a simple time domain signal with a zoomed in view of the first 32^{nd} of the traces on the right. The top trace is the input signal. The middle trace is its autocorrelation. The bottom trace maintains a part of the autocorrelation result deemed important. To compute the bottom trace, the input was subsampled by 8 in the Fourier domain, multiplied by its conjugate, and inverse transformed. To facilitate plotting, the trace was padded with zeros.

Frequency domain subsampling the inputs is not the identical operation to time windowing the inputs due to the periodicity of the DFT. In fact, late time arrivals in the input will be aliased into the early time of the records. Therefor, windowing the output of correlation aliases the time domain of the input.

It is more efficient to alias the time domain by summing in time rather than decimating the frequency axis. Further, windowing in time avoids wrap-around problems for the output, which is why only a factor of 8 decimation could be supported rather than 32 for Figure 2. If a long trace $f(t)$ is broken into J short sections of the same length $g_j(t)$, the DFT for a particular ω,

$$F|_\omega = \mathrm{DFT}[\,f(t)]|_\omega = \frac{1}{\sqrt{n}}\sum_t f(t)\mathrm{e}^{-i\omega t}\,, \tag{2}$$

results in

$$\mathrm{DFT}[\,f(t)]|_\omega = J^{-3/2}\sum_{j=1}^{J}\mathrm{DFT}[g_j(t)]|_\omega = J^{-3/2}\mathrm{DFT}[\sum_{j=1}^{J} g_j(t)]|_\omega\,, \tag{3}$$

provided only that the sampling theorem permits the particular ω to be commonly supported by the two transforms. Thus the beginning lags of a long correlation can be computed by first stacking time records (of length desired for the output, t), or subsampling the Fourier domain. More important is the demonstration that windowing the output of a long correlation aliases, or stacks, the time domain of the input.

If the component functions $g_j(t)$ are shot gathers from $R(\mathbf{x}_r,\mathbf{x}_s,t)$, we can see that the long signal $f(t)$ is $R(\mathbf{x}_r,t*n_s)$ where n_s is the number of shots in the survey. For transmission wavefields, the time axis and the shot axis are naturally combined. If we assume that individual sources, and their reflections that occur t seconds afterward, are distributed at intervals within the total recording time τ, field data is $T_{field}(\mathbf{x}_r,\tau)$ where $\tau = t*n_s +$ wait-time.

Without knowing when sources happen, and acknowledging that multiple sources may fire within time t, equation 1 will be practically implemented

$$\begin{aligned} R(\mathbf{x}_r,t) &= \\ &= -\frac{1}{2}\Re\left\{\rho_f\left(\mathrm{alias}[T(\mathbf{x}_r,\tau),t]\right)\right\} \\ &= -\mathrm{rect}\left(\frac{max(t)}{2\tau}\right)\frac{1}{2}\Re\left\{\rho_f[T(\mathbf{x}_r,\tau)]\right\} \\ &= \sum_{\mathbf{x}_s} R(\mathbf{x}_r,\mathbf{x}_s,t). \end{aligned} \tag{4}$$

Above, ρ_f is the autocorrelation function, alias$[T,t]$ is either frequency subsampling or summation of constituent time windows to return records of length t, τ is the total recording time, and

$$\mathrm{rect}(x) = \begin{cases} 1 & \text{for} \quad |\mathrm{x}| < 1/2 \\ 0 & \text{for} \quad |\mathrm{x}| > 1/2 \end{cases}.$$

This formulation recognizes the sum over the shot axis inherent in processing the long recording of the entire experiment instead of windows around known arrivals. Summing time windows, equation 4, is the fastest way to calculate $R(\mathbf{x}_r, t)$, by saving a possibly very long DFT, with no loss of accuracy.

The implicit aliasing in equation 4 sums the wavefields from multiple sources. The sources may be naturally aliased as well if they are not sufficiently separated in time. Define the transmission wavefields from individual sources $a(\mathbf{x}_r, t)$ and $b(\mathbf{x}_r, t)$. When placed randomly on the field record, $T(\tau) = a\mathrm{e}^{i\phi_a} + b\mathrm{e}^{i\phi_b}$. Correlation by equation 4 yields

$$TT^* = aa^* + bb^* + ab^*\mathrm{e}^{i(\phi_a - \phi_b)} + ba^*\mathrm{e}^{i(\phi_b - \phi_a)} \,. \tag{5}$$

The sum of the first two terms is the result dictated by equation 1. The second two are extra. If $\phi_a + t < \phi_b$, one term will be acausal, and the other the accumulation of late-time correlations that can be windowed away. If $\phi_b < \phi_a + t$, they will be included in the correlated gathers. Redefine a and b as the impulse response of the earth, I_e, convolved with source functions, f, now containing their phase delays ϕ. As such, the cross-terms of equation 5 in the Fourier domain are

$$ab^* = (f_a I_e)(f_b I_e)^* = f_a f_b^* I_e^2 = f_c I_e^2 \,. \tag{6}$$

Like the first two terms in equation 5, the cross-terms do have the desired information about the earth. However, the source function f_c it is convolved with is not zero phase. If the source functions are random series, the $f_c I_e^2$ terms within the gathers will decorrelate and diminish in strength as the length of f and the number of cross-terms increases. However, their inclusion violates the definition of $R(\mathbf{x}_r, \mathbf{x}_s, \omega)$. Also, while we may hope to collect a large number of sources, it is probably unreasonable to expect many of them to have great length.

Figure 3 shows the effect of the cross terms expanded in equation 6. This figure was produced with exactly the same processing sequence as Figure 2, but with an input signal less craftily manufactured. The model for the signal in both figures is three subsurface sources under a single reflector.

The timing of the sources in Figure 2 was carefully controlled such that direct arrivals were at samples $1,512$, and 2048. This contrivance allows the summing of constituent windows 256 or 512 samples long while maintaining zero phase. The second source in Figure 3 arrives at the receiver before the reflection from the first source. The third source is randomly placed at the far end of the trace. Neither version of the autocorrelation, middle and bottom traces, looks like the desirable results in Figure 2. If sources fire within the same time window, their superposition is the ramification of the cross-terms acquired with equation 4.

If shots are summed from different locations, the effect is the production of gathers with a single source function with areal extent instead of a spatial impulse. The sum of an impulse at every surface location builds a horizontal planewave source in 3D (given flat geography). Summing all available shot-gathers builds a zero offset data volume, $\mathbf{h} = 0$, given good lateral coverage of zero phase source functions.

Without predefining the zero time for each source, stacking at zero time is impossible. The sum of these sources synthesizes one with some topography instead of a simple plane. For impulsive sources, the combined shape would be the surface defined by the locations of the minimum time (top of the hyperbola) of the first arrival from each source. This superposition of plane waves will yield reflections at more than one angle or offset, but likely limited to near zero.

Therefore, equation 4 creates a volume of data with the same kinematics as reflection data collected with a single source that is an unknown superposition of planewaves. The unknown, areal, source function is in the data, but the approximation from equation 1 to equation 4 produces a data volume that should not be treated as conventional impulsive-source seismic.

MIGRATION

Migration produces a subsurface image, as a function of space, from many seismic experiments collected on a convenient datum (usually the surface of the earth). Each shot collected in a survey carries redundant information about subsurface reflectors. Collapsing this redundancy to specific locations in the subsurface makes a structural image beneath the survey. For this reason, the words imaging and migration are used interchangeably. Within the geophysical literature, any debate around the migration of active seismic data focuses around which particular implementation is appropriate for specific problems and holds that the process is almost mandatory in all but the most simple geology.

I will briefly describe the steps of shot-profile wave-equation depth migration in order to see how mapping the transmission response to the reflection response can be satisfied therein. Of the many migration strategies available, this discussion centers on the ability of shot-profile migration to simultaneously satisfy the correlation required for passive imaging while providing the acknowledged benefits of a migrated image space. To begin, it is useful to think of depth migration as a cascade of constituent parts: extrapolation, and imaging.

Extrapolation

The hyperbolic wave equation describes the propagation of seismic energy through a medium. The scalar simplification of the equation describes the propagation of compressional waves through an acoustic medium. While this simplification is not necessary, it is an established, robust, and convenient framework for this discussion.

With the eikonal solution to the wave equation, a wavefield is extrapolated from an initial condition to a close approximation of its state at a different location or time. Claerbout (1971) explains the details and derivation of the mathematics.

Despite the fact that energy within the medium freely propagates in all directions, the Fourier solution to the wave equation can most easily be implemented as the cascade of two phase-shift operators that both handle lateral propagation, while individually accounting for either positive or negative propagation in a third dimension. These are the unitary, causal and acausal SSR (Single Square Root) operators, so named after their form

$$\text{SSR}^{+1} = \mathrm{e}^{-ik_z \Delta z} \quad \text{and} \quad \text{SSR}^{-1} = \mathrm{e}^{+ik_z \Delta z} \tag{7}$$

where

$$k_z = \sqrt{(\omega s)^2 - k_{\mathbf{x}}^2}\,. \tag{8}$$

In the above equations, Δz is the depth interval across which we are extrapolating the data, k_z is the wavenumber in the depth direction, $k_{\mathbf{x}}$ is the horizontal wavenumber calculated from the data, and s is the provided slowness model of the subsurface. Because the SSR is a unitary operator[1], conjugation changes its propagation direction from causal to acausal or vice versa. These simple operators are precise for only laterally invariant media. More advanced propagators are extensively discussed in the literature, and do not change the discussion herein. Such higher order operators should be used in practice.

These extrapolation operators are used in shot-profile migration by a double extrapolation process to approximately reverse the seismic experiment. The up-coming energy of single a shot-gather, $U_{z=0}$, is the k_{th} shot-gather from the total reflection experiment located at $\mathbf{x}_{s_k}$:

$$U_{z=0}(\mathbf{x}_r; \mathbf{x}_{s_k}, \omega) = R(\mathbf{x}_r, \mathbf{x}_s = \mathbf{x}_{s_k}, \omega). \tag{9}$$

Each gather is iteratively extrapolated by SSR^{-1} to all desired deeper levels $z > 0$ with a supplied

[1]This is strictly true only for propagating wavefields. Non-propagating harmonics, or standing waves, would cause a problem, but are not recorded by the geophones.

subsurface velocity model

$$U_{z+1}(\mathbf{x}_r;\mathbf{x}_{s_k},\omega) = \mathrm{SSR}^{-1}U_z(\mathbf{x}_r;\mathbf{x}_{s_k},\omega). \tag{10}$$

The phase-shift of the SSR subtracts time from the beginning of the experiment in order to model the wavefield as if it were collected at a deeper level.

The down-going energy for a particular shot is a modeled wavefield, $D_{z=0}(\mathbf{x}_r;\mathbf{x}_{s_k},\omega)$, of zeros with a single trace source wavelet (at time zero) at the source location $\mathbf{x}_{s_k}$. This wavefield is extrapolated with the causal phase-shift operator SSR^{+1} through the velocity model to all desired levels $z > 0$

$$D_{z+1}(\mathbf{x}_r;\mathbf{x}_{s_k},\omega) = \mathrm{SSR}^{+1}D_z(\mathbf{x}_r;\mathbf{x}_{s_k},\omega). \tag{11}$$

The phase-shift adds time to the onset of experiment corresponding to the travel time required for the energy of the source to reach progressively deeper levels of the earth. If an areal source, such as a length of primachord or 30 Vibroseis trucks, were used instead of a point source, $D_{z=0}$ should be modeled to reflect the appropriate source function.

This double extrapolation process is performed for each individual shot experiment to all depth levels interest. Instead of reducing the complexity and volume of the original data, the process greatly increases the volume by maintaining the separation of up-coming and down-going energy through all depth levels for all time for all the receivers recording each shot. To produce a subsurface image, the energy in these wavefields must be combined.

Imaging

The imaging aspect of migration compares the energy in the D and U wavefields at each subsurface location to output a single subsurface model. The operator used to accomplish this goal is called the

imaging condition. While different migration schemes require subtly different imaging conditions, the following discussion focuses on the one required for shot-profile depth migration.

Reflectors are correctly located in the image, $i_z(\mathbf{x},\mathbf{h})$, at every depth level z as a function of horizontal position, $\mathbf{x}$, and offset, $\mathbf{h}$, when energy in the two wavefields is collocated in both space and time. This condition maps energy to the image when the source has reached the location where a reflection was produced. This is carried out by extracting the zero time-lag of the (spatially lagged) cross-correlations of the traces in the two wavefields. Last, the entire model space is populated by summing the results of all the images produced in this manner by each shot collected in the survey (Rickett and Sava, 2002)

$$i_z(\mathbf{x},\mathbf{h}) = \delta_{\mathbf{x},\mathbf{x}_r} \sum_{\mathbf{x}_{s_k}} \sum_{\omega} U_z(\mathbf{x}_r + \mathbf{h}; \mathbf{x}_{s_k}, \omega) D_z^*(\mathbf{x}_r - \mathbf{h}; \mathbf{x}_{s_k}, \omega) \,. \tag{12}$$

The Kronecker delta function indicates that the surface coordinates of the wavefields, $\mathbf{x}_r$, are also used for the image, and * represents conjugation. Notice that the zero lag of the correlation is calculated by summing over frequency. The inclusion of subsurface offset, $\mathbf{h}$, shows the general applicability for non-zero offset, which is explained in the reference above.

In total, migration requires

- extrapolating up-coming shot-gathers acausally through the velocity model,
- extrapolating down-going source functions causally through the velocity model,
- correlating the two wavefields at all depth levels,
- extracting the zero lag coefficient of the correlation, and
- summing the results of all individual shots.

Direct migration of transmission wavefields

Having explained the two processes, extrapolation and imaging, required for migration, I now return to the manipulation of transmission wavefields. Artman and Shragge (2003) shows the applicability of direct migration for transmission wavefields. Artman et al. (2004) provides the mathematical justification for $h = 0$, zero phase source functions.

The matrix form of correlation of two equilength signals in the Fourier domain has one signal along the diagonal of a square matrix multiplied by the second signal vector. Extrapolation in the Fourier domain is also a diagonal square matrix where the values of the diagonal are the phase shifts calculated for each wavenumber in the wavefield. Circular correlation and extrapolation are both linear square operators. As such, the two operations are commutable. This means that the correlation required to calculate the earth's reflection response from transmission wavefields can be performed after extrapolation as well as at the acquisition surface.

Using equation 4 to correlate field data (not being able collect T as a function of individual source functions), we cannot process the result of the correlation with all available reflection migration data tools. Without knowing the exact timing of all the source functions, it is not possible to completely eliminate all time delays. However, the autocorrelation of field data can still be migrated with a scheme that includes extrapolation and a correlation imaging condition. Shot-profile depth migration is the most common algorithm to be defined by these two features.

Migration produces the correct image if the source wavefield, D, is correct for the data wavefield, U. Shot-profile migration becomes planewave migration if all shot-gathers are summed for wavefield U, and a horizontal plane source is modeled for wavefield D. Wave-equation extrapolators are correct for any initial conditions provided by the user. The information lost in this sum is the redundancy across the offset axis. Without the need for AVO (amplitude variation with offset), or MVA (migration

shot-profile migration, $\mathbf{h}=0$				passive imaging		
$\left(\sum_{\mathbf{x}_{s_k}} U_{z=0}(\mathbf{x}_r;\mathbf{x}_{s_k},t)\right)$	$\otimes$	$\left(\sum_{\mathbf{x}_{s_k}} D_{z=0}(\mathbf{x}_r;\mathbf{x}_{s_k},t)\right)$	$=$	$T_{z=0}(\mathbf{x}_r,t)$	$\otimes$	$T_{z=0}(\mathbf{x}_r,t)$
$\vert$		$\vert$		$\vert$		$\vert$
SSR^{-1}		SSR^{+1}		SSR^{-1}		SSR^{+1}
$\downarrow$		$\downarrow$		$\downarrow$		$\downarrow$
$U_{z=1}(\mathbf{x}_r,t)$	$\otimes$	$D_{z=1}(\mathbf{x}_r,t)$	$=$	$T^{-}_{z=1}(\mathbf{x}_r,t)$	$\otimes$	$T^{+}_{z=1}(\mathbf{x}_r,t)$

Figure 1.

velocity analysis), this information is not required, and the $h=0$ image is satisfactory. As such, calculating i_z from equation 12 as a function of subsurface offset, **h**, is likely a wasted effort without first convolving the data with various planewaves as mandated for a complete planewave migration (Sun et al., 2001; Liu et al., 2002).

A transmission wavefield is the superposition of U and D. Figure 4 pictorially demonstrates how direct migration of passive seismic data fits into the framework of shot-profile migration to produce the 0^{th} and 1^{st} depth levels of the zero offset image. Moving the sum over shots in the imaging condition of equation 12 to operate on the wavefields rather than their correlation, changes shot-profile migration to planewave migration. The sum over frequency has been omitted to reduce complexity. To complete the migration to the deepest level of interest, the cascade of extrapolations and correlations will continue for all z required. Importantly, after the first extrapolation step, with the two different phase-shift operators, the two transmission wavefields are no longer identical, and can be redefined U and D. This is noted with superscripts on the T wavefields at depth.

Extrapolating the transmission wavefield with a causal phase-shift operator models the propagation of energy reflecting from the free-surface that is the source function for later reflections. Extrapo-

lating the transmission wavefield with an acausal phase-shift operator models the reverse-propagation of energy through the subsurface that carries the information about the layers below. Even if this information is embedded in an odd wavelet, the physics that migration is trying to reverse remains the same.

The shot-profile migration imaging condition performs the passive seismic correlation at every depth level in the model. In effect, the extrapolation step re-datums the experiment to successively deeper levels in the subsurface at which the wavefields are correlated. Simultaneously, the extraction of the zero time-lag for the image discards energy in the two wavefields that is not collocated. This includes energy that has been extrapolated in the wrong direction (since the same data is used for both at first). Conveniently, the only modification needed to make a conventional shot-profile migration program into a passive imaging program is to copy the input data wavefield into the memory location of the source wavefield which is usually zeros seeded with a wavelet.

Image space vs. data space trace density

The image produced from a migration enjoys a more dense areal coverage than the acquisition geometry. As the number of receivers gets small, the (noisy) correlated shot-gathers may have too few traces to allow identification of coherent events. Increased trace density of the migrated image can help ameliorate this problem. The justification for this claim can be afforded through two arguments.

First, the aliasing criteria established in Zhang et al. (2003) dictates that the output of a wave-equation depth migration should have twice finer areal sampling than the acquisition. This is due to the correlation in the imaging-condition of equation 12. While performing a time correlation of the traces, there is an implicit multiplication of the space axes. A seismic signal extracted across the

traces can be represented as some accumulation of periodic functions, the identity

$$2\cos[k_1 x]\cos[k_2 x] = \cos[(k_1+k_2)x] + \cos[(k_1-k_2)x]$$

with arbitrary wavenumbers k_i, dictates that the output space should be twice finer sampled than the input signals. The first term on the RHS can appropriately carry two times higher wavenumber energy than either input function. This mandates a finer sampling for the result. Alternatively, if one is familiar with time migrations where resorting to *midpoint-offset* coordinates is required, it is obvious that a midpoint exists half-way between each source/receiver location given equal sampling of source and receiver.

Second, if zero-traces are included between live traces, the wave-equation extrapolator will fill energy across the gaps in the course of the migration by wave-front healing. As energy is extrapolated to depth, it is also moved laterally. After a few extrapolation steps, the energy on the live traces constructively interferes to 'heal' the wavefront, while artifacts loose energy and dissipate. Because this process needs sufficient extrapolation steps to be beneficial, the migration can suffer at shallow depths until the series of impulses has crossed the zero traces to become a wavefront.

EXAMPLES WITH SYNTHETIC DATA

To demonstrate the processing explained above, several synthetic acoustic passive data sets were generated. Transmission wavefields from 225 impulsive sources across the bottom of a velocity model were propagated with a two-way extrapolation program. To then simulate a passive recording campaign, a unique source function was convolved with each wavefield before summing all of them together. The length of the source function trace mimics the duration of the recording campaign. The shape, location, and duration of the wavelet used within the source function trace reflects the nature of the ambient subsurface noise field.

The source functions incorporate many of the features of the toy trace in Figures 2 & 3. Each source can unexpectedly explode at any time, and sources will have a wavelet with a finite length coda. Each finite length source function is then parameterized as a scaled wavelet, of some duration, randomly placed within an empty trace whose length reflects the total recording time of the experiment.

Figure 5 shows synthetic data from a model containing two diffractors. Panel (a) is a transmission wavefield from a source on the far left of the model, while the source in panel (b) was at $x = 5000m$. Sources were parameterized as bandlimited wavelets $0.05s$ long placed on the time axis to align their direct arrivals. Panel (c) is the sum all 225 similar wavefields from different shots. The coherent summation of the direct arrivals makes a strong planewave at $t \sim 0.6s$, and the diffractors are well captured.

In contrast, Figure 4 shows synthetic data from a the same model with two diffractors with the addition of random phase delays for the source functions throughout the experiment. Panel (a) is a transmission wavefield from a source beneath $x = 1200m$, while the source in panel (b) was at two-thirds of the way across. Panel (c) is the sum of all 225 similar wavefields from different shots. The strong planewave and coherent diffractors from Figure 5 have been replaced by an uninterpretable superposition. These data after correlation will not be migrated correctly with methods demanding impulsive sources at zero time.

Data was also synthesized through a model containing two synclines. Figure 6 shows summed wavefields with, panel (a), and without, panel (b), correcting for the onset time of the 225 subsurface sources. Panel (b) has been truncated from $32s$. Bandlimited impulses were used as sources without any addition of randomness. Figure 7 shows zero offset images produced by direct migration of the data shown in Figure 6. All frequencies were used from a $32s$ length experiment. Panel (b) is

not as high quality as panel (a). This could be in part from events wrapping around the time axis when applying their respective phase delays. A faint reflection mimicking the first event can be seen at $z = 350m$. This could be a manifestation of the aphysical events at late lag which have not been windowed away. Given the dramatic departure of the data (panel (b), Figure 6) from a horizontal planewave source, significant energy may also be at $\mathbf{h} \neq 0$. The most obvious difference is the diminution of the multiple from the first reflector at $z = 485$. The second reflector is much clearer in panel (b) without its interference.

Increasing the signal to noise ratio

Very important among the motivations for migrating passive seismic data, is the need to increase the signal to noise ratio of the output. If the experiment records only a small amount of energy, the synthesized data from correlation can be completely uninterpretable. The correlated gather in the left panel of Figure 8 has a few events centered around $4000m$, but is dominated by noise. In fact, this gather is full of useful energy hidden by the random source functions that the data were produced with.

Draganov et al. (2004) systematically explores the quality of a passive seismic processing effort as a function of the number of subsurface sources, the length of assumed source functions, and migration. That work and Rickett and Claerbout (1996) identify increasing the signal-to-noise ratio by the familiar $1/\sqrt{\xi}$ factor where ξ can be time samples in the source function, or number of subsurface sources captured in the records. Also, migrating the passive data was able to produce interpretable images from data sets that showed little to no continuity in the correlated gathers.

The direct controls available to increase quality of passive seismic effort are the length of time data is collected, and the number of receivers fielded for the experiment. If the natural rate of seismic-

ity within a field area is constant, accumulation of sufficient signal dictates how long to record. Not surprisingly, increasing the total length of time of the source traces for the synthetic data described above does not change the quality of the output. If all the sources are used with the same source functions, this only adds quiet waiting time between the events that contributes neither positively nor negatively to the output. This experiment implies a changing rate of seismicity. When interpreting the increase in signal by factor $1/\sqrt{t}$ with application to short subsurface sources, t represents the mean length of the source functions rather than total recording time. Assuming some rate of subsurface sources associated with each field site, the total recording time will control the quality of the output by $1/\sqrt{s}$ where s is the number of sources captured.

Another method to increase the quality of the experiment is to migrate more traces. Migration facilitates the constructive summation of information captured by each receiver in the survey. Therefore, more receivers sampling the ambient noisefield results in more constructive summation to each image location in the migrated image. In this manner migration increases the signal-to-noise ratio of a subsurface reflection by the ratio $1/\sqrt{r}$, where r is the number of receivers that contain the reflection. This allows the production of very interpretable images despite the raw data or correlated gathers showing little promise.

The right panel of Figure 8 shows an image produced with the 32 seconds of passive data directly migrated. An identical image was produced with only every 16^{th} frequency and is not shown. The correlated gather in the panel to the left was produced with the same data. The source functions used were each random, but were allowed only maximum length of $3.0s$. By combining the weak redundant signal within that gather with all of the others through migration produces a spectacular result.

FIELD EXPERIMENT

Cross-correlating seismic traces of passively collected wavefields has a rich history pertaining to the study of the sun (Duvall et al., 1993). On earth thus far, only two dedicated field campaigns to test the practicality of passive seismic imaging can be found in the literature: Baskir and Weller (1975), and Cole (1995). Neither experiment produced convincing results. With the hope that hardware limitations or locality could explain these previous experiments, I conducted a shallow, meter(s) scale, passive seismic experiment in the summer of 2002. 72 $40Hz$ geophones were deployed on a $25cm$ grid on the beach of Monterey Bay, California linked to a Geometrics seismograph. The experiment was combined with an active investigation of the same site using the same recording equipment and a small hammer (Bachrach and Mukerji, 2002). A short length of $15cm$ diameter plastic pipe was buried a bit less than one meter below the surface. The array was approximately 100 meters from the water's edge. The water table is approximately three meters deep. The velocity of the sand, derived from the active survey, was a simple gradient of 180 to $290m/s$ from the surface to the water table, and then $1500m/s$.

Figure 9 shows the time-migrated active source image with a clear anomaly associated with the hollow pipe and the water table. A simple RMS gradient velocity to the water table was used for imaging. The high quality of the beach sand allowed usable signal to as high as $1200Hz$ for that survey.

Passive data was collected over the course of two days two weeks later. Due to the limitations of the recording equipment, only one hour of data exist from the campaign. The seismograph was only able to buffer several seconds of data in memory before writing to a file. The time required to write, reset and re-trigger happened to be about 5 times greater than the length of data captured depending on sample rates. Data was collected at several sampling rates. Through the course of the

experiment, we found it possible to fly a small kite (plastic grocery bag) that would continuously move the triggering wire over the hammer plate to trigger the system automatically as soon as it was ready to record. The individual records were then spliced together along the time axis to produce long traces. The gaps in the traces do not invalidate the assumptions of the experiment as long as the individual recordings are at least as long as the longest two-way travel time to the deepest reflector.

Because the array was only eight by nine stations, shot-gathers produced by correlation, even when resampled as a function of radial distance from the center trace, had too few traces to find consistent events. Migrating the data, as described above, provides both signal to noise enhancement, as well as interpolation. In this case, five empty traces were inserted between the geophone locations for processing as shown in Figure 10.

Data were collected to correspond to distinct environmental conditions through the course of the experiment. Afternoon data was collected during high levels of cultural activity and wind action. Night data had neither of these features, while morning data had no appreciable wind noise. In all cases the pounding of the surf remained mostly consistent. By processing data within various time windows, it was hoped that images of the water table at different depths could be produced. However, given the $2m$ maximum offset of the array, ray parameters less than 17^{o} from the vertical would be required to image the a $3m$ table reflector at the very center of the array. Very little energy was captured at such steep incidence angles. Had we not been so careful not to walk around the array during recording, this might not have been the case.

Figures 11-13 show the images produced during the different times of the day. Approximately five minutes of 0.001 seconds/sample data were used to produce each image by direct migration. Usable energy out to $450Hz$ is contained in all the data collected. Abiding by the $1/4$ wavelength rule, and using $200m/s$ with $400Hz$, the data should resolve targets to $\sim 0.125m$. Other data volumes

corresponding to various faster and slower sampling rates were processed, though these results are the most pleasing.

Pre-processing in most cases consisted of a simple bandpass to eliminate electrical grid harmonics, as the higher octaves carry any useful signal considering the low velocity of the beach sand and the small areal extent of the array. Figure 11 is the image produced mid-day. The two panels are the x and y sections corresponding to the center of the pipe. Figure 12 was produced with data from around midnight. The image planes are the same as for the previous figure. One dimensional spectral whitening was also tried, though the simple application remained stable only during the night acquisition. Figure 13 was produced with the whitened version of the data used for the previous figure. Notice the instability at shallow depths before the wavefront healing has interpolated across the empty traces. Data collected in the morning did not yield appreciably different images from the night data to warrant inclusion.

All output images contain an appreciable anomaly at the location of the buried pipe. Complicating the interpretation of the results, the ends of the pipe were not sealed before burial. After two weeks under the beach, it is impossible to know how much of the pipe was filled, which would destroy the slow, air-filled target. Future experiments would also incorporate target with a severe angle that could clearly stand out.

In the whitened night data image and the bandpassed day data image, there is hint of a reflector at depth that could be the water table. High tide on that day was at 4:30 in the afternoon, and fell to low tide at about 8:30pm, and thus the relative change of this hint of a reflector is consistent. However, due to the limitations of the array discussed above, and the lack of strength and continuity along the cross-line direction, I do not hold this to be a very reliable interpretation.

CONCLUSION

Definitive parameters for the numbers of geophones required, and sufficient length of time to assure quality results for a passive seismic experiment are ongoing research topics as few field experiments have yet been analyzed. It is clear however, that an over-complete sampling of the surficial wavefield is required, and that the length of time required will be dictated on the activity of the local ambient noise field. Considering the layout of equipment, over-complete sampling means that more receivers are better, and areal arrays will be much better than linear ones. This can be understood by considering a plane-wave propagating along an azimuth other than that of a linear array. After the direct arrival is captured, the subsequent reflection path pierces the Earth's surface again in the cross-line direction away from the array. With a 2.5D approximation, the apparent ray parameter of the arrival will suffice given an areally consistent and planar source wave. Because the true direct arrival associated with a reflection travel-path was not recorded, the possibility of erroneous phase delays and wavelets could distort the result.

Processing windowed subsets of a passive survey may be advantageous. If time-localized events are present, such as teleseismic arrivals, one can process smaller time windows when sure of significant contribution to the image. Without knowledge of if or how many sources are active within the bulk of the data, long correlations of the raw data are an almost inevitable approximation, equation 4, to the rigorous derivation, equation 1. Fortunately, first aliasing the short time records reduces the computation cost for a DFT by $1/n_\tau$ where n_τ is the number of samples in the long input trace. n_τ will be $O(10^7)$ for just one day of data collected at $0.004s$ sampling rate. In practice, the length of the aliased windows should probably be several times as long as the minimum time to the deepest reflector. Multiple sources within this time are handled perfectly by direct migration, and the risk of adding the end of the reflection series to the beginning of the record will be minimized. The decision

can be determined by whatever compute resources are available for the size of the data set collected.

The inherent aliasing within the approximation sums the source functions within the output. This superposition of sources does not produce $R(\mathbf{x}_r, \mathbf{x}_s, \omega)$ under realistic situations. Instead the result is, $\sum_{\mathbf{x}_s} R(\mathbf{x}_r, \mathbf{x}_s, \omega)$. This data volume can only be migrated with an algorithm that can accept generalized source functions (parameterized by space and time), and uses a correlation imaging condition. Both of these conditions are enjoyed by shot-profile migration.

Migrating all sources at the same time removes the redundant information from a reflector as a function of incidence angle. This makes velocity updating after migration impossible. At this early stage, I contend that passive surveys will only be conducted in actively studied regions where very good velocity models are already available. If this becomes a severe limit, the incorporation of planewave migration strategies can fill the offset dimension of the image.

Finally, moving the modeling of the reflection response from the transmission response down to the image point during migration also introduces the possibility for more advanced imaging conditions, such as deconvolution, and other migration strategies, such as converted mode imaging.

Acknowledgments

Thanks to my colleagues and advisors at Stanford University for insightful discussions and development of the infrastructure to perform these experiments. I thank Deyan Draganov of Delft University for successful collaboration and his modeling efforts. Ran Bachrach provided the Michigan State shallow seismic acquisition equipment for the beach experiment as well as his image from his active seismic experiment. Emily Chetwin and Daniel Rosales helped collect data on the beach. Partial funding for this research was enjoyed from NSF award 0106693, Petroleum Research Fund grant ACS PRF#37141 -AC 2, and the Stanford Exploration Project.

REFERENCES

Artman, B., and Shragge, J., 2003, Passive seismic imaging: AGU Fall Meeting, Eos Transactions of the American Geophysical Union, Abstract S11E–0334.

Artman, B., Draganov, D., Wapenaar, C., and Biondi, B., 2004, Direct migration of passive seismic data: 66th Conferance and Exhibition, EAGE, Extended abstracts, P075.

Bachrach, R., and Mukerji, T., 2002 AGU Fall Meeting, Eos Transactions of the American Geophysical Union, Abstract T22B–1141.

Baskir, C., and Weller, C., 1975, Sourceless reflection seismic exploration: Geophysics, **40**, 158.

Claerbout, J. F., 1968, Synthesis of a layered medium from its acoustic transmission response: Geophysics, **33**, no. 2, 264–269.

Claerbout, J. F., 1971, Toward a unified theory of reflector mapping: Geophysics, **36**, no. 03, 467–481.

Cole, S. P., 1995, Passive seismic and drill-bit experiments using 2-D arrays: Ph.D. thesis, Stanford University.

Derode, A., Larose, E., Campillo, M., and Fink, M., 2003, How to estimate the green's function of a heterogeneous medium between two passive sensors? application to acoustic waves: Applied Physics Letters.

Draganov, D., Wapenaar, K., and Thorbecke, J., 2004, Passive seismic imaging in the presence of white noise sources: The Leading Edge, **23**, no. 9, 889âĂŞ892.

Duvall, T., Jefferies, S., Harvey, J., and Pomerantz, M., 1993, Time-distance helioseismology: Nature, **362**, 430–432.

Liu, F., Stolt, R., Hanson, D., and Day, R., 2002, Plane wave source composition: An accurate phase encoding scheme for prestack migration: Soc. of Expl. Geophys., 72nd Ann. Internat. Mtg, 1156–1159.

Rickett, J., and Claerbout, J., 1996, Passive seismic imaging applied to synthetic data: Stanford Exploration Project - Annual Report, **92**, 83–90.

Rickett, J. E., and Sava, P. C., 2002, Offset and angle-domain common image-point gathers for shot-profile migration: Geophysics, **67**, no. 03, 883–889.

Schuster, G., Yu, J., Sheng, J., and Rickett, J., 2004, Interferometric/daylight seismic imaging: Geophysics Journal International, **157**, 838–852.

Sun, P., Zhang, S., and Zhao, J., 2001, An improved plane wave prestack depth migration method: Soc. of Expl. Geophys., 71st Ann. Internat. Mtg, 1005–1008.

Wapenaar, K., Thorbecke, J., and Draganov, D., 2004, Relations between reflection and transmission responses of three-dimensional inhomogeneous media: Geophysical Journal International, **156**, 179–194.

Zhang, Y., Sun, J., and Gray, S., 2003, Aliasing in wavefield extrapolation prestack migration: Geophysics, **68**, no. 2, 629–633.

Zhang, L., 1989, Reflectivity estimation from passive seismic data: Stanford Exploration Project-Annual Report, **60**, 85–96.

LIST OF FIGURES

random source functions of various lengths. Right: Zero offset migration of the data from the left panel produced by direct migration.

9 In-line, x, and cross-line, y, time migrated active seismic image. The hollow pipe causes an over-migrated anomaly at 12ms, 19m in the inline (X) direction. A strong water table reflection is imaged at 28ms. After Bachrach, 2003.

10 A small time window of in-line and cross-line sections of a raw passive transmission wave-field inserted on a five times finer grid for migration.

11 Migrated image from passive data collected during the windy afternoon. In-line and cross-line depth section extracted at the coordinates of the buried pipe.

12 Migrated image from passive data collected during the night. In-line and cross-line depth section extracted at the coordinates of the buried pipe.

13 Migrated image from passive data collected during the night. One dimensional spectral whitening applied before migration to the same raw data used in Figure 12. In-line and cross-line depth section extracted at the coordinates of the buried pipe.

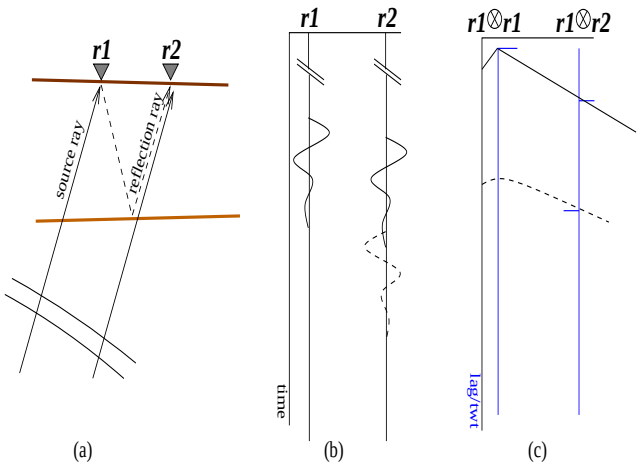
r1
r2
source ray
reflection ray
(a)
r1
r2
time
(b)
r1⊗r1
r1⊗r2
lag/twt
(c)

Figure 1.

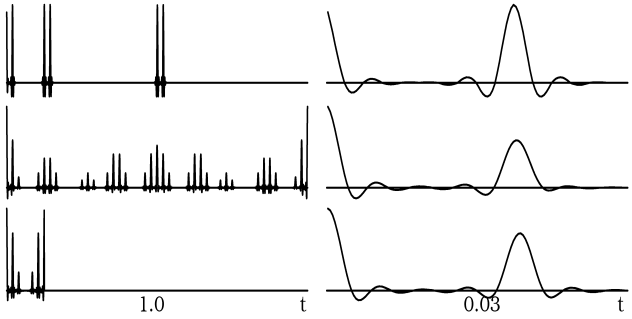

Figure 2.

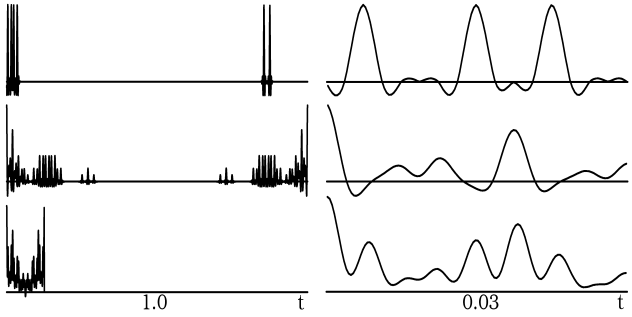

Figure 3.

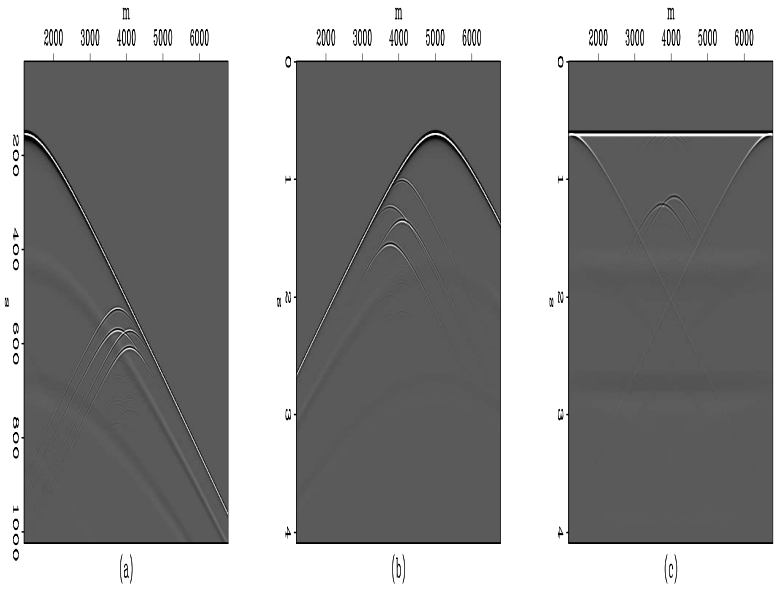

Figure 4.

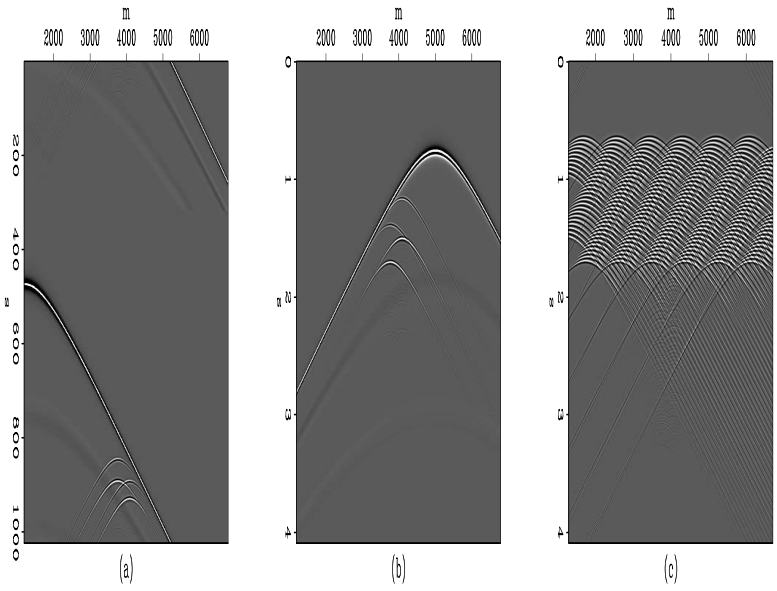

Figure 5.

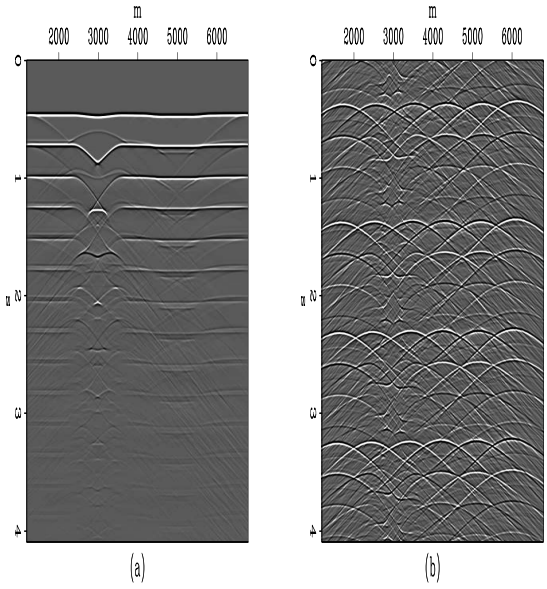

Figure 6.

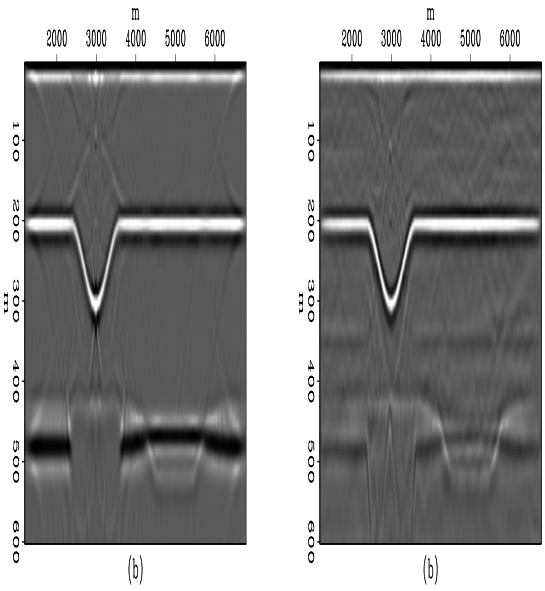
m
2000
3000
4000
5000
6000
100
200
300
400
500
600
m
(b)
m
2000
3000
4000
5000
6000
100
200
300
400
500
600
m
(b)

Figure 7.

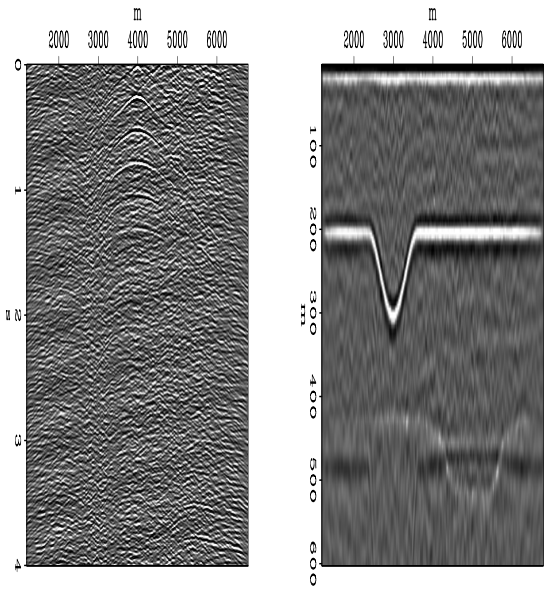
m
2000
3000
4000
5000
6000
0
1
2
3
4
s
m
2000
3000
4000
5000
6000
100
200
300
400
500
600
ms

Figure 8.

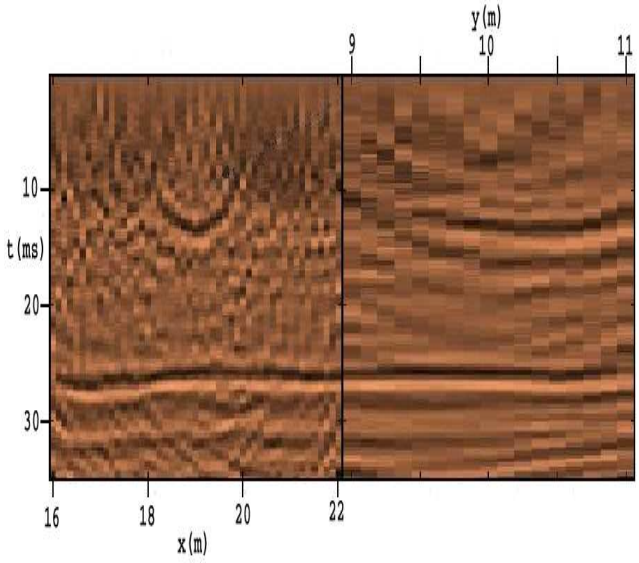

Figure 9.

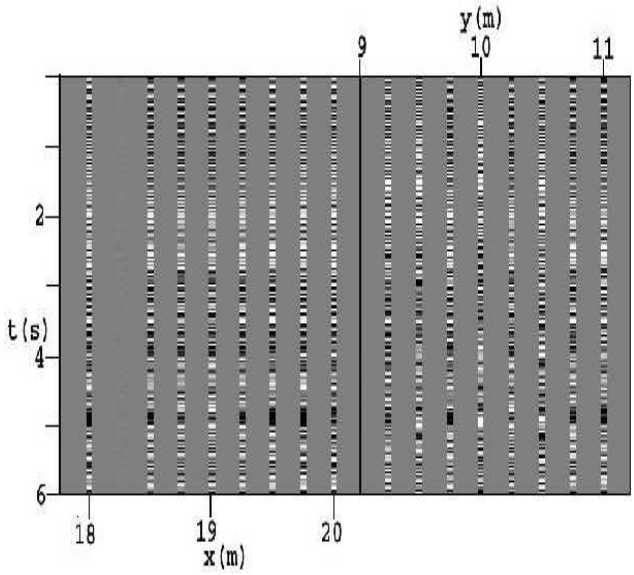

Figure 10.

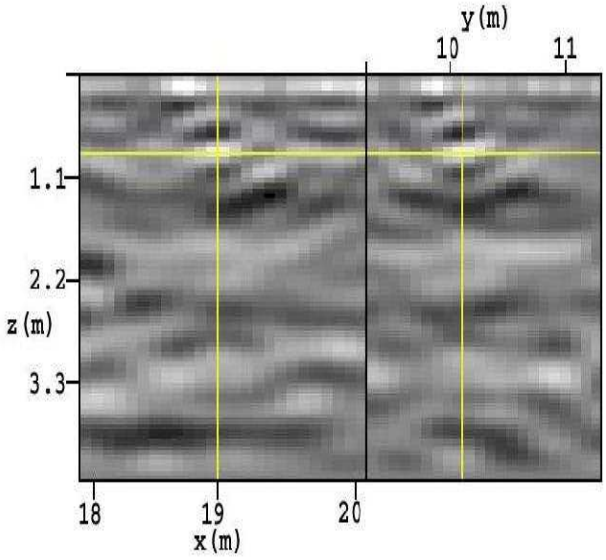

Figure 11.

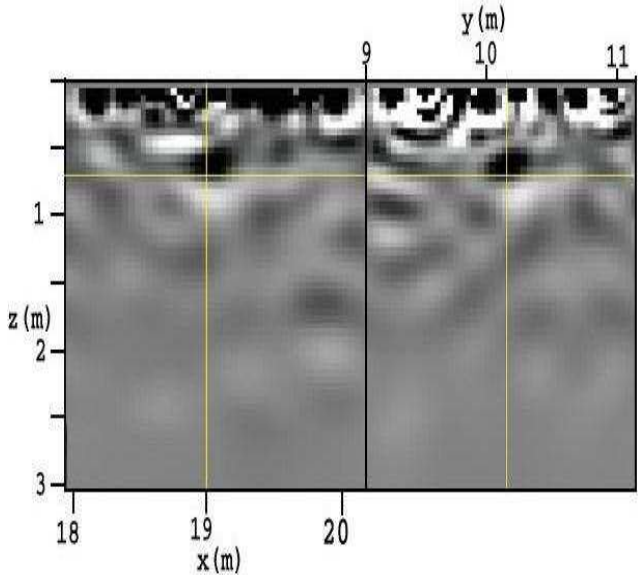

Figure 12.

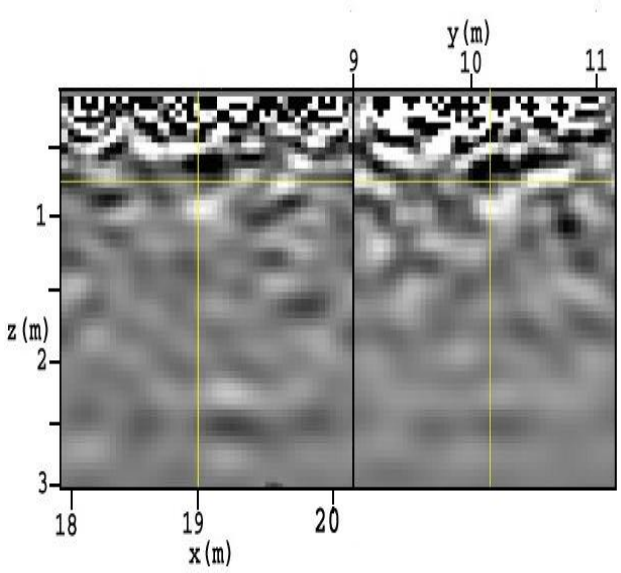

Figure 13.